Sensorless Control of Permanent Magnet Synchronous Motor in Full Speed Range*

Dingdou Wen, *Wei Wang and Yang Zhang**
(School of Electrical and Information Engineering, Hunan University of Technology, Zhuzhou 412008, China)

Abstract: Aiming at resolving the limitation of the speed regulation range of sensorless control technology, a new composite sensorless control strategy is proposed to realize a control method for a permanent magnet synchronous motor (PMSM) in full speed range. In the medium- and high-speed range, the improved new sliding mode observer method is used to estimate the motor speed and rotor position information. In the zero and low speed range, in order to avoid the defects of the sliding mode method, the rotating high-frequency voltage signal injection method is used. When switching between low, medium, and high speed, the fuzzy control algorithm is adopted to achieve smooth transitions. The simulation experiment results show that the hybrid mode combining the sliding mode observer and rotating high-frequency voltage injection methods, can effectively reduce the jitter in the algorithm switching process, and realize the smooth control of a PMSM in full speed range.

Keywords: PMSM, full speed range, rotating high-frequency voltage signal injection method, sliding mode observer method, fuzzy control

1 Introduction

Permanent magnet synchronous motor (PMSM) is widely used in the small and medium power ranges because of its excellent attributes such as high reliability, small size, high efficiency, and energy saving characteristics. However, there are few studies on the full speed range of the motor. At present, full-speed sensorless control methods can be roughly divided into two categories: the first class of methods uses a combination of open-loop startup and back-EMF (Electromotive force) observation, and the second class of methods uses a combination of high-frequency injection and back-EMF observation. The former uses constant current frequency conversion or constant voltage frequency conversion, drags the motor open loop to a certain speed, and switches to a closed loop control, based on back-EMF observation [1]. The methods in this group are simple to control, but the low-speed dynamic performance is not high. Devices that have high requirements for low-speed dynamic performance, adopt the second class of methods to achieve sensorless control over the full speed range [2].

Accurate detection of the motor speed and rotor position information in the low-speed range, realized by the characteristics of the rotor salient pole, does not rely on the fundamental wave equation. The method of applying an externally excited high-frequency voltage signal to the stator winding of the motor is adopted; the high frequency response current generated by the voltage signal, can be processed to extract the required detection signal [3]. The medium- to high-speed range usually uses the position estimation algorithm for back-EMF observation [4]. Commonly used methods include extended Kalman filtering, model reference adaptation, and the sliding mode observer [5]. The rational design of the observer can meet the requirements of speed

Manuscript received July 23, 2021; revised November 23, 2021; accepted December 15, 2021. Date of publication June 30, 2022; date of current version April 3, 2022.
* Corresponding Author, E-mail: hut_zy@163.com
* Supported by the National Natural Science Foundation of China (51907061) and Natural Science Foundation of Hunan Province (2018JJ2100, 2019JJ50119).
Digital Object Identifier: 10.23919/CJEE.2022.000018

regulation and loading performance in the medium- and high-speed ranges. Compared with other methods, the sliding mode observer method is robust and computationally simple and hence, widely used [6]. At the same time, in order to achieve sensorless control in the full speed range, it is necessary to develop a strategy to attain smooth switching between the high-speed injection method used during low and medium speed operation and the sliding mode observer method using during high speed operation.

Most of the high-speed and low-speed switching methods use a weighted average and a hysteresis smooth switching strategy [7-8]. The weighted average method is relatively simple; however, when the given speed happens to be in the transition interval, it may cause frequent switching between the two methods, which will cause the speed fluctuation to be large and unstable; the latter method is more complicated and difficult to achieve in practical applications. Therefore, it is key to a reliable operation to realize a smooth switching strategy for full speed sensorless control.

2 Mathematical model of PMSM

Regardless of the phenomenon of motor saturation [9], the voltage equation of PMSM in rotating coordinates is expressed as follows

$$\begin{bmatrix} u_d \\ u_q \end{bmatrix} = \begin{bmatrix} R_s + L_d p & -\omega_e L_q \\ \omega_e L_d & R_s + L_q p \end{bmatrix} \begin{bmatrix} i_d \\ i_q \end{bmatrix} + \omega_e \psi_f \begin{bmatrix} 0 \\ 1 \end{bmatrix} \tag{1}$$

where u_d, u_q, i_d, i_q are the voltage and current in the d-q (two-phase rotor rotation axis) system, R_s is the stator resistance, p is the differential operator, L_d, L_q are the stator inductance, ω_e is the rotor electrical angular velocity, and ψ_f is the permanent magnet flux linkage.

The d-q axis of electromagnetic torque is established as follows

$$T_e = \frac{3}{2} p_n i_q \left(\psi_d i_q - \psi_q i_d \right) \tag{2}$$

where ψ_d, ψ_q are the equivalent values of the permanent magnet flux linkage under the shaft system, and p_n is the motor pole pairs.

The switch to the static coordinate system is expressed as follows

$$\begin{bmatrix} u_\alpha \\ u_\beta \end{bmatrix} = R_s \begin{bmatrix} i_\alpha \\ i_\beta \end{bmatrix} + \frac{\mathrm{d}}{\mathrm{d}t} \begin{bmatrix} \psi_\alpha \\ \psi_\beta \end{bmatrix} \tag{3}$$

where

$$\begin{bmatrix} \psi_\alpha \\ \psi_\beta \end{bmatrix} = \begin{bmatrix} L - \Delta L\cos(2\theta) & \Delta L\sin(2\theta) \\ \Delta L\sin(2\theta) & L + \Delta L\cos(2\theta) \end{bmatrix} \bullet \frac{\mathrm{d}}{\mathrm{d}t} \begin{bmatrix} i_\alpha \\ i_\beta \end{bmatrix} + \psi_f \begin{bmatrix} \cos\theta \\ \sin\theta \end{bmatrix} \tag{4}$$

and where $\Delta L = \left(L_d - L_q \right) / 2$ 、 $L = \left(L_d + L_q \right) / 2$ are the d-q axis inductance mean, and difference, respectively.

3 Sensorless compound control strategy

3.1 Medium- and high-speed control based on improved sliding mode observer

The mathematical model of PMSM in the α-β coordinate system is expressed as follows

$$\begin{cases} \dfrac{\mathrm{d}i_\alpha}{\mathrm{d}t} = -\dfrac{R}{L} i_\alpha - \dfrac{1}{L} K_e e_\alpha + \dfrac{1}{L} u_\alpha \\ \dfrac{\mathrm{d}i_\beta}{\mathrm{d}t} = -\dfrac{R}{L} i_\beta - \dfrac{1}{L} K_e e_\beta + \dfrac{1}{L} u_\beta \end{cases} \tag{5}$$

where u_α, u_β, i_α, i_β, e_α, e_β are the voltage, current, and back electromotive force on the α-β axes, respectively, R is phase resistance, L is phase inductance, and K_e is the back-EMF coefficient.

The back-EMF model of PMSM in the α-β axes is expressed as follows

$$\begin{bmatrix} e_\alpha \\ e_\beta \end{bmatrix} = E_{ex} \begin{bmatrix} -\sin\theta_e \\ \cos\theta_e \end{bmatrix} \tag{6}$$

where $E_{ex} = \left(L_d - L_q \right) \left(\omega_e i_d - \dot{i}_q \right) + \omega_e \psi_f$.

From Eq. (6), the back-EMF contains motor speed and rotor position information. The sliding mode observer equation is expressed as follows

$$\begin{cases} \dfrac{\mathrm{d}\hat{i}_\alpha}{\mathrm{d}t} = -\dfrac{R}{L} \hat{i}_\alpha + \dfrac{u_\alpha}{L} - \dfrac{K}{L} sign\left(\overline{i}_\alpha \right) \\ \dfrac{\mathrm{d}\hat{i}_\beta}{\mathrm{d}t} = -\dfrac{R}{L} \hat{i}_\beta + \dfrac{u_\beta}{L} - \dfrac{K}{L} sign\left(\overline{i}_\beta \right) \end{cases} \tag{7}$$

where $\hat{i}_\alpha$, $\hat{i}_\beta$ are the current observation, $\overline{i}_\alpha$, $\overline{i}_\beta$ are

the current observation error, and K is the sliding mode coefficient.

The sliding mode variable structure with function switching control is expressed as follows

$$u = u_{eq} + Ksign\left(s\left(x\right)\right) = e + Ksign\left(s\left(x\right)\right) \quad (8)$$

When the system switches to the synovial state, $s\left(x\right)=0$, $\frac{\mathrm{d}}{\mathrm{d}t}s\left(x\right)=0$. After a limited interval, $\overline{i}_{\alpha}=0$, $\overline{i}_{\beta}=0$. Assume $\frac{\mathrm{d}}{\mathrm{d}t}\overline{i}_{\alpha}=0$, $\frac{\mathrm{d}}{\mathrm{d}t}\overline{i}_{\beta}=0$. The equation is expressed as follows

$$\begin{cases} u_{eq\alpha} = \left[Ksign\left(\overline{i}_{\alpha}\right)\right]_{eq} = e_{\alpha} \\ u_{eq\beta} = \left[Ksign\left(\overline{i}_{\beta}\right)\right]_{eq} = e_{\beta} \end{cases} \quad (9)$$

The estimated values of rotor position and speed are expressed as follows

$$\begin{cases} \hat{\theta}_{\alpha} = \dfrac{\omega_s}{s+\omega_s} e_{\alpha} \\ \hat{\theta}_{\beta} = \dfrac{\omega_s}{s+\omega_s} e_{\beta} \end{cases} \quad (10)$$

In order to weaken the inherent chattering phenomenon of the sliding mode observer [10], the S function is now used to replace the switching function as follows

$$\begin{bmatrix} \Gamma_{\alpha} \\ \Gamma_{\beta} \end{bmatrix} = \begin{bmatrix} \Gamma\left(\hat{i}_{\alpha} - i_{\alpha}\right) \\ \Gamma\left(\hat{i}_{\beta} - i_{\beta}\right) \end{bmatrix} = \begin{bmatrix} \dfrac{1}{1+\exp\left[-n\left(\hat{i}_{\alpha} - i_{\alpha}\right)\right]} - \dfrac{1}{2} \\ \dfrac{1}{1+\exp\left[-n\left(\hat{i}_{\beta} - i_{\beta}\right)\right]} - \dfrac{1}{2} \end{bmatrix} \quad (11)$$

where Γ_{α}、Γ_{β} are the components of the S function on the α-β axes. The S function curve is shown in Fig. 1.

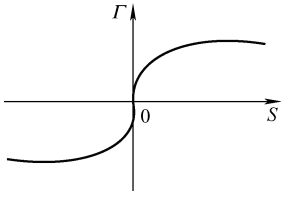

Fig. 1 S function curve

During the actual operation of PMSM, the flux linkage will change under the influence of various factors, such as load and ambient temperature, which affects the estimation accuracy of the rotor position [11]. In this paper, a phase-locked loop is designed, and the feedback of the S function is introduced into the observer. The block diagram of the improved sliding mode observer is shown in Fig. 2.

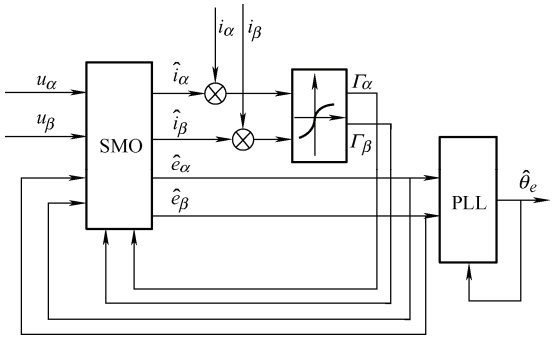

Fig. 2 Schematic diagram of improved sliding mode observer

From Eq. (7)

$$\hat{\theta}_e = -\arctan\left(\frac{\hat{e}_{\alpha}}{\hat{e}_{\beta}}\right) \quad (12)$$

The motor speed information can be obtained by Eq. (13)

$$\hat{\omega}_e = \frac{\mathrm{d}\hat{\theta}_e}{\mathrm{d}t} \quad (13)$$

The low-pass filter present in the device will inevitably cause a phase delay and result in certain error when calculating the speed of the PMSM, which affects the stability of the system. To compensate for the phase delay, a phase-locked loop (PLL) is embedded in the speed position calculation section to make the PMSM operation more stable. The block diagram of the PLL is shown in Fig. 3.

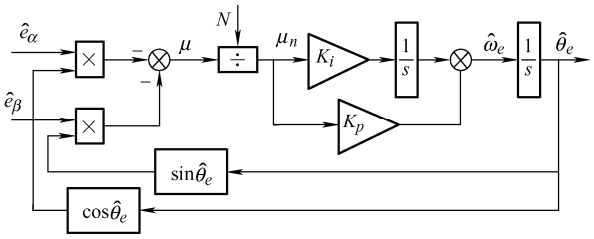

Fig. 3 Block diagram of PLL structure

where K_p, K_i are PLL ratio and integral coefficients.

$$N = -\sqrt{\hat{e}_{\alpha}^{\,2} + \hat{e}_{\beta}^{\,2}} \quad (14)$$

$$\mu = -\hat{e}_\alpha \cos\hat{\theta}_e - \hat{e}_\beta \sin\hat{\theta}_e \tag{15}$$

Substituting Eq. (6) into Eq. (15)

$$\mu = -E_{ex} \sin\left(\hat{\theta}_e - \theta_e\right) \tag{16}$$

$$\mu_n = \frac{\mu}{N} = \sin\left(\hat{\theta}_e - \theta_e\right) \tag{17}$$

When the estimated rotor position of the PMSM and the actual rotor position are infinitely close, then that is the position error and is expressed as follows

$$\mu_n \approx \hat{\theta}_e - \theta_e \tag{18}$$

The back-EMF error is

$$\begin{cases} \overline{e}_\alpha = -\omega_e \overline{e}_\beta - \dfrac{m}{k}\dfrac{1}{L_d}\overline{e}_\alpha \\ \overline{e}_\beta = -\omega_e \overline{e}_\alpha - \dfrac{m}{k}\dfrac{1}{L_d}\overline{e}_\beta \end{cases} \tag{19}$$

where m, k are the gain of the sliding mode observer.

By solving the differential equation of Eq. (19) and using Laplace transformation, the eigenvalues are obtained as follows

$$s_{1,2} = \frac{-m/k \pm jL_d\omega_e}{L_d} \tag{20}$$

The two characteristic roots of the equation are complex and conjugate. Therefore, the system converges.

3.2 Low-speed control based on high-frequency voltage injection method

When a high-frequency signal is injected, its frequency is much higher than the inherent frequency of the motor, and the influence of the voltage drop on the stator resistance of the PMSM, and the induced electromotive force, can be ignored. The stator voltage equation is expressed as follows

$$\begin{bmatrix} u_\alpha \\ u_\beta \end{bmatrix} \approx \begin{bmatrix} P & 0 \\ 0 & P \end{bmatrix} \begin{bmatrix} \psi_\alpha \\ \psi_\beta \end{bmatrix} \tag{21}$$

After injecting a high-frequency sinusoidal voltage signal, the voltage equation generated in the α-β coordinate system can be expressed as

$$\begin{bmatrix} u_{\alpha i} \\ u_{\beta i} \end{bmatrix} = U_i \begin{bmatrix} \cos(\omega_i t) \\ \sin(\omega_i t) \end{bmatrix} = U_i \exp(j\omega_i t) \tag{22}$$

where U_i is the amplitude of the injected high-frequency signal, ω_i is the angular frequency of the high-frequency signal, and $\omega_i \geqslant \omega_r$.

The high-frequency response current equation is expressed as follows

$$\begin{bmatrix} \dfrac{\mathrm{d}i_{\alpha i}}{\mathrm{d}t} \\ \dfrac{\mathrm{d}i_{\beta i}}{\mathrm{d}t} \end{bmatrix} = \begin{bmatrix} L + \Delta L\cos(2\theta) & \Delta L\sin(2\theta) \\ \Delta L\sin(2\theta) & L - \Delta L\cos(2\theta) \end{bmatrix}^{-1} \begin{bmatrix} u_{\alpha i} \\ u_{\beta i} \end{bmatrix} \tag{23}$$

Integrating and simplifying using Eq. (22)

$$\begin{bmatrix} i_{\alpha i} \\ i_{\beta i} \end{bmatrix} = \frac{U_i}{\omega_i\left(L^2 - \Delta L^2\right)} \begin{bmatrix} L\sin(\omega_i t) + \Delta L\sin(2\theta - \omega_i t) \\ -L\cos(\omega_i t) - \Delta L\cos(2\theta - \omega_i t) \end{bmatrix} \tag{24}$$

The negative phase sequence, owing to the high-frequency current response, contains rotor position information. It is necessary to use a band-pass filter to filter out signals other than the injected high-frequency signals, and then filter the positive-phase sequence component to the opposite of the negative phase sequence component in the carrier current through a synchronous axis high-pass filter (SFF). The high-frequency current vector is transformed through a series of coordinates of the SFF. At this point, the positive-phase sequence high-frequency current vector becomes DC, and the positive sequence component in the high-frequency current signal can be filtered by a general high-pass filter.

Multiplying Eq. (24) by the conversion factor at the same time

$$i_{in} = I_{in} \exp\left[j\left(2\theta - 2\omega_i t + \frac{\pi}{2}\right)\right] \exp(j\omega_i t) = I_{in} \exp\left[j\left(2\theta - \omega_i t + \frac{\pi}{2}\right)\right] \tag{25}$$

where $I_{in} = \dfrac{U_i}{\omega_i}\left[\dfrac{-\Delta L}{L^2 - \Delta L^2}\right]$.

The error signal of rotor information obtained by the heterodyne method is expressed as follows

$$\varepsilon = i_{\alpha in}\cos\left(2\hat{\theta}-\omega_i t\right)+i_{\beta in}\cos\left(2\theta-\omega_i t\right)= I_{in}\sin\left(2\hat{\theta}-2\theta\right) \tag{26}$$

where ε is the loop filter PI regulator input, $\Delta\theta=\hat{\theta}-\theta$, when $2\theta\leqslant\frac{\pi}{6}$, $\sin 2\Delta\theta\approx 2\Delta\theta$.

$$\varepsilon \approx 2I_{in}\Delta\theta \tag{27}$$

The heterodyne method can be used to obtain a tracking error signal proportional to the phase error [12]. As long as the tracking error signal is adjusted to approach zero, the rotor position estimation angle is guaranteed to be close to the actual value.

3.3 Sensorless control under compound strategy

In view of the limitations of the current low and medium to high-speed switching control algorithms, a single-point fuzzy control method [13] is proposed to realize the smooth switching of the PMSM from low speed to medium and high speed.

3.3.1 Traditional compound control strategy

At present, the most commonly used traditional compound algorithm is the weighted average algorithm. The principle diagram of weighted switching is shown in Fig. 4.

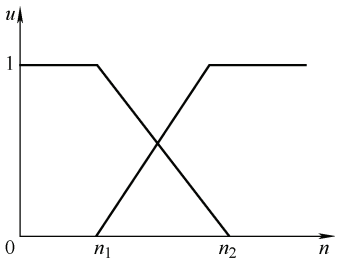

Fig. 4 Schematic diagram of weighted switching

When the estimated speed of the PMSM is greater than the upper limit speed n_2, the sliding mode observer method is used. When the estimated speed of the motor is less than the lower limit speed n_1, the rotating high-frequency voltage injection method is expressed as follows

$$u=\begin{cases}0 & n<n_1\\ \dfrac{n_2-n}{n_2-n_1} & n_1\leqslant n\leqslant n_2\\ 1 & n>n_2\end{cases} \tag{28}$$

where u is the weighting factor, and n is the estimated rotational speed of the system composite observer.

The system block diagram of this weighted switching is shown in Fig. 5.

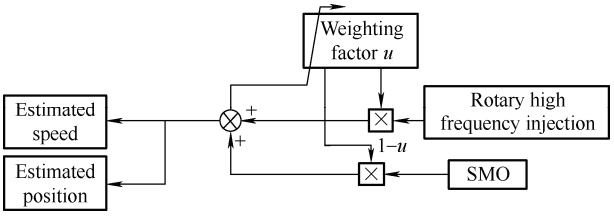

Fig. 5 Block diagram of fuzzy control strategy

The input of the weight coefficient adjustment rule is the speed error ε and the error rate of change ε_r. The total output of the control system can be expressed as follows

$$n=un_{hf}+(1-u)n_{smo} \tag{29}$$

$$\theta=u\theta_{hf}+(1-u)\theta_{smo} \tag{30}$$

where n_{hf} is the rotational high-frequency voltage injection method to estimate the speed, n_{smo} is the sliding mode observer to estimate the speed, θ_{hf} is the rotating high-frequency voltage injection method to estimate the angle, and θ_{smo} is the estimated angle of the sliding mode observer, n_{hf} / θ_{hf}.

3.3.2 Weight coefficient fuzzy control

The idea of the fuzzy weighting coefficient [14-15] is that at different stages of the adjustment process, the weighting coefficient u is adjusted according to the change of the input error ε, and the PMSM is smoothly switched from low speed to medium and high speed.

The various aspects that are involved in weight coefficient fuzzy control include the following. The fuzzification process performs functions or table look-up calculations. This paper adopts the function calculation method, which not only makes the calculation uncomplicated, but also simplifies the process of compiling the table. Suppose that the input error is ε and the error change rate is ε_c, then its membership functions are as shown in Fig. 6, respectively.

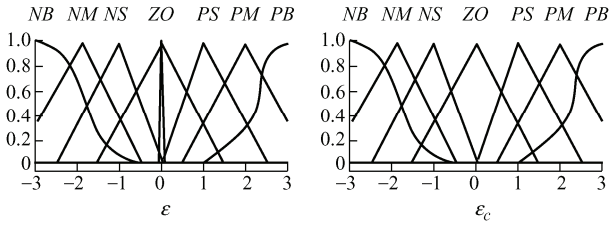

Fig. 6 Input membership function

Now the weight domain u of the system is set to [0, 1], and the values are taken according to 11 levels: $u_1, u_2, \cdots, u_{11}$. Subsequently, its membership function is represented by a single point as shown in Fig. 7.

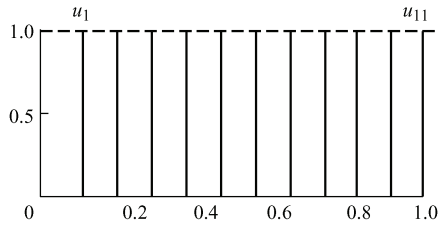

Fig. 7 Weight coefficient u membership function

(2) Input quantity synthesis algorithm. This is applied to find the membership value of the antecedent of each rule. Commonly used methods are OR, AND, and algebraic equations. In this paper, the AND method is selected. Therefore, the membership value of the antecedent of each rule can be expressed as

$$\omega = \min\left\{u(\varepsilon), u(\varepsilon_c)\right\} \tag{31}$$

(3) Inference rules. The adjustment of the weighting coefficient should follow this rule: in the initial stage of the switching interval, the estimated error ε is very large, and PB (positive big) and ε_r are very small, and the value of u is almost 0. At this time, the main role of the rotating high-frequency voltage injection method is: as the speed increases, ε is ZO (zero), but ε_r is NB (negative big) or PM (positive middle), indicating that the system is in the middle of an adjustment period, and the weight coefficient is adjusted appropriately; when ε and ε_r are gradually reduced, in order to avoid impact on the dynamic performance of the system, u should be gradually increased; in the late adjustment period, the output approaches the target, and u should continue to increase; when both ε and ε_r are zero, u = 1 is the largest, and the speed and rotor position information sensors are sliding mode observers, thus achieving motor speed, and the position is switched between the rotating high-frequency injection method and the sliding mode observer.

Applying the aforementioned principles and the values of the corresponding periods ε and ε_r in Fig. 10, 49 control rules for the weight coefficient u can be obtained, as shown in Tab. 1.

Tab. 1 Control rules for weight coefficients

	C						
E	*NB*	*NM*	*NS*	*ZO*	*PS*	*PB*	*PM*
	Weights u						
NB			u_1				
NM		u_4		u_5	u_6		
NS	u_4		u_8			u_6	
ZO		u_7	u_{10}		u_{10}		u_3
PS				u_9	u_8	u_7	
PM	u_3	u_6	u_6				u_4
PB					u_1	u_4	

According to these rules, the weight coefficient u look-up table can be obtained through an offline fuzzy operation. When the system is running, the controller has a quantized value of $\varepsilon(k)$ and $\varepsilon_c(k)$.

(4) Deblurring [13]. This article uses the center of gravity method as the final output of fuzzy reasoning.

$$u = \frac{\int U\mu(U)\mathrm{d}u}{\int \mu(U)\mathrm{d}u} \tag{32}$$

3.3.3 Simulation analysis of full-speed range compound sensorless control method

Generally, the best switching point is at 10%-20% of the rated speed of the motor. In this study, the speed switching range is set at 150-300 r/min, which is simulated under Matlab/Simulink, as shown in Fig. 8.

The relevant parameters of PMSM used in the simulation are shown in Tab. 2.

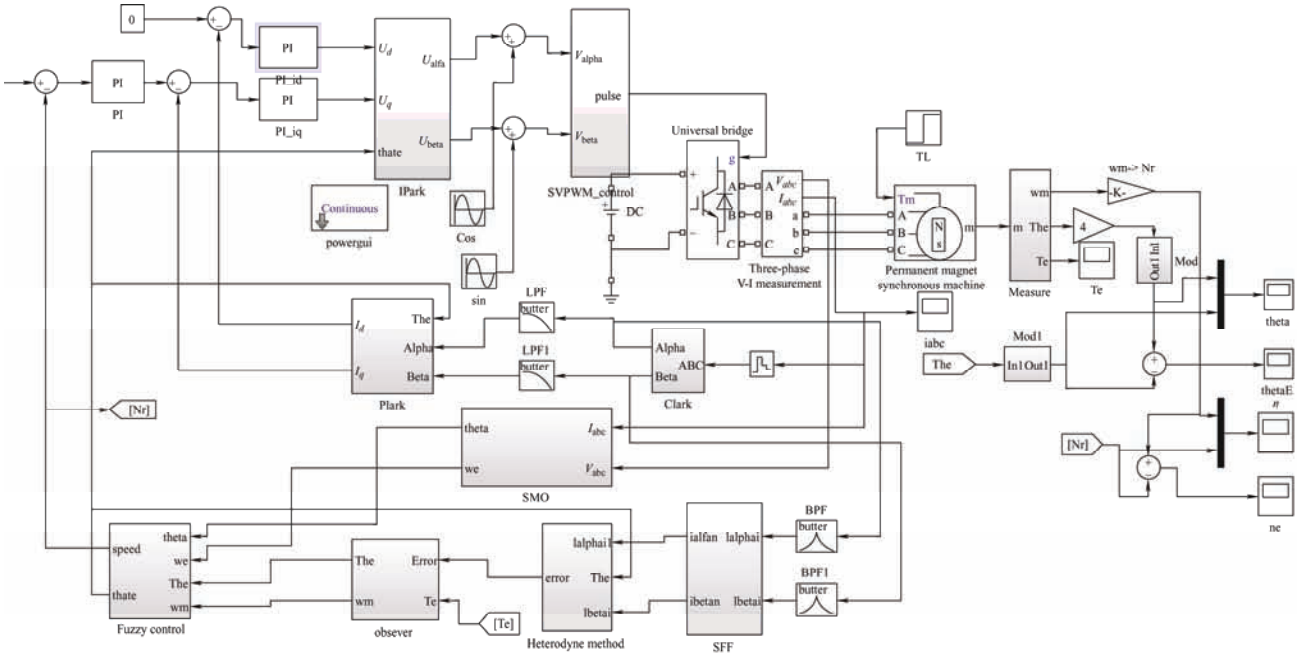

Fig. 8 Simulation diagram of full range sensorless control based on fuzzy control

Tab. 2 Parameters of PMSM

Parameter	Value
Rated power/kW	1.4
Stator resistance/Ω	0.8
Rated speed/(r/min)	1 500
d-axis inductance/H	0.008
q-axis inductance/H	0.021
Rotor flux linkage/Wb	0.175
Inertia/(kg·m^2)	0.000 46
Number of pole-pairs	2

(1) When the motor runs from low speed to medium and high speed, we can set the speed switching interval to [150, 300], and observe the simulation results of the traditional weighted switching control system.

According to Fig. 9a, when the motor has just started, it runs at 50 r/min with no load at first, and adds half a load after 0.3 s. After 0.6 s, it starts to enter the traditional weighting mode. At 1.4 s, the motor is fully loaded and then it stabilizes. However, from the enlarged switching range in Fig. 9b, when 4 N • m load is added at the beginning of switching from low speed to medium and high speed, there is a jump in speed, and when switching to sliding mode control, the overshoot is about 50 r/min. It can be seen from Fig. 9c that, after entering the speed switching interval, there is a certain error in the rotor position.

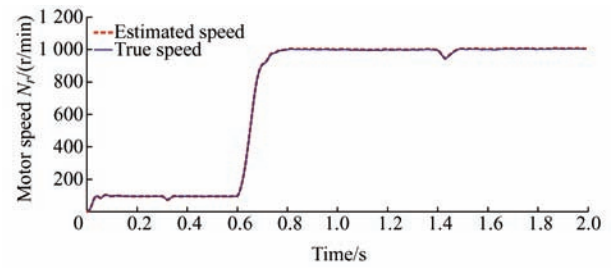

(a) Full range speed response curve of traditional weighted switching control

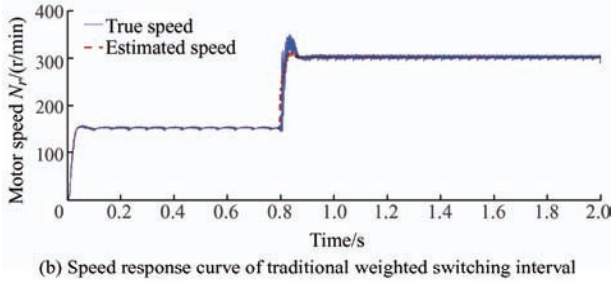

(b) Speed response curve of traditional weighted switching interval

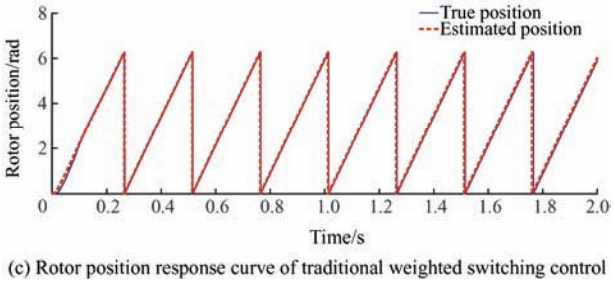

(c) Rotor position response curve of traditional weighted switching control

Fig. 9 The full range sensorless control waveform under the traditional weighting algorithm

(2) Under the same working conditions as the traditional algorithm, use of fuzzy control based on the speed and rotor position waveform in the switching interval.

According to Fig. 10a, the actual and estimated speeds are smooth and the response speed is fast. From the enlargement of the switching interval in Fig. 10b, when the same load as in the traditional algorithm is added to the fuzzy control algorithm, and is switched, the motor speed is smoother, and no large oscillation occurs, compared with the traditional switching algorithm,. It can be seen from Fig. 10c that this method can smoothly enter the rotation speed switching interval, and has good tracking dynamic performance.

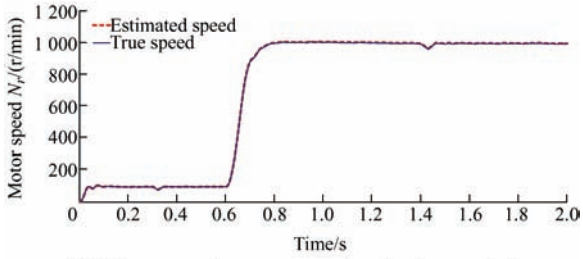

(a) Full range speed response curve based on fuzzy control

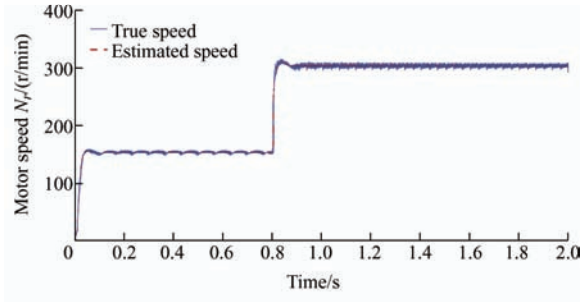

(b) Speed response curve of switching interval based on fuzzy control

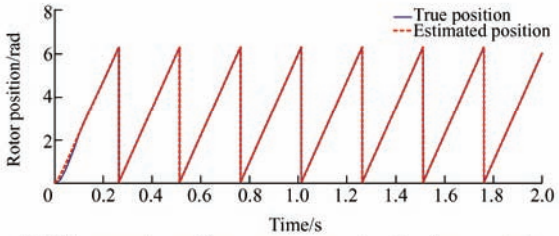

(c) Full range rotor position response curve based on fuzzy control

Fig. 10 Full range sensorless control waveform based on fuzzy control

(3) Error waveform comparison in the switching interval between the traditional weighted switching and fuzzy control when the motor is running in the full speed range, based on the speed and rotor position.

According to Figs. 11a and 11b, when entering the switching interval at 0.6 s, it can be seen that the error of the traditional weighted switching speed increases significantly, up to about 55 r/min. Through fuzzy control, it can be seen that the speed and speed errors of the two algorithms during switching, are significantly smaller.

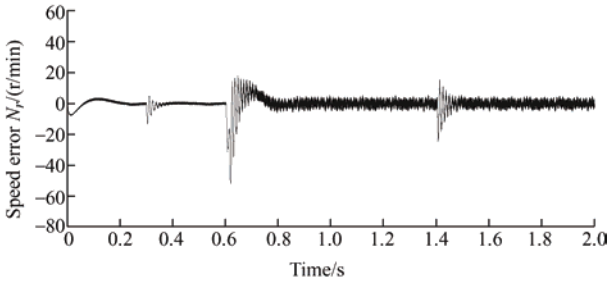

(a) Full range speed error curve based on traditional weighted switching control

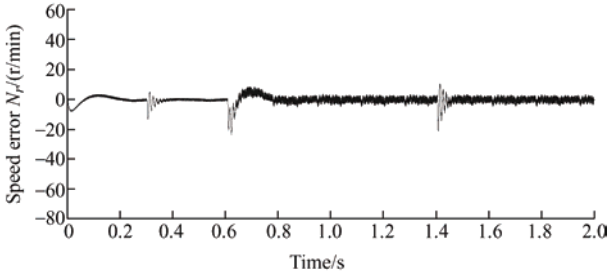

(b) Full range speed error curve based on fuzzy control

Fig. 11 Comparison of the speed waveforms of the two control algorithms in the switching interval

According to Fig. 12a and 12b, when entering the switching interval at 0.6 s, it can be seen that the error of the traditional weighted switching rotor is significantly increased. Through fuzzy control, it can be seen that the two algorithms can effectively and accurately detect the rotor position during the switching process.

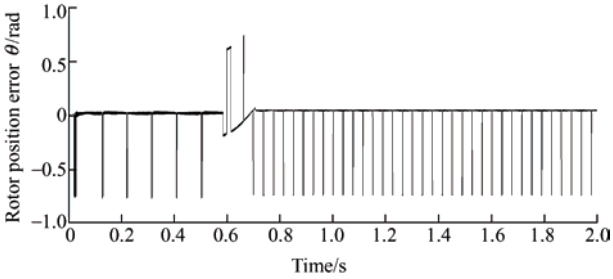

(a) Full range rotor position error curve based on traditional weighted switching control

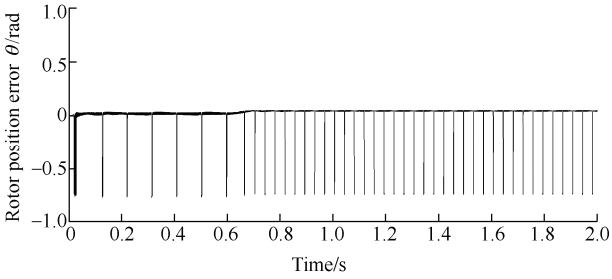

(b) Full range rotor position error curve based on fuzzy control

Fig. 12 Comparison of the rotor position waveforms of the two control algorithms in the switching interval

4 Experimental results and analysis

The experimental platform, which employs two

permanent magnet synchronous motors, a PMSM as the load, and a digital signal processor (DSP-TMS320F28335) controller, is shown in Fig. 13. The parameters of PMSM are given in the simulation.

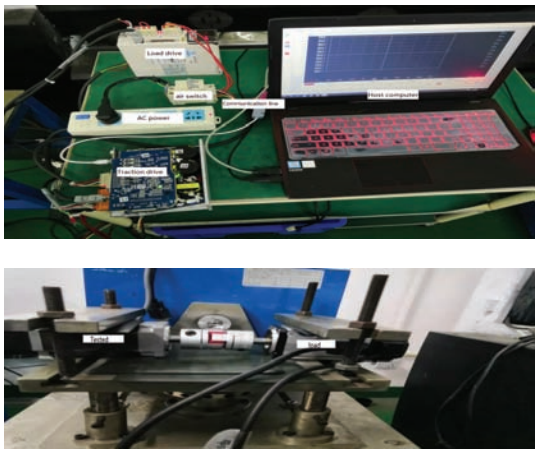

Fig. 13 Experimental platform

(1) When the motor runs from low speed to medium and high speed, we set the speed switching interval to [150, 300]. The experimental results are shown in Fig. 14.

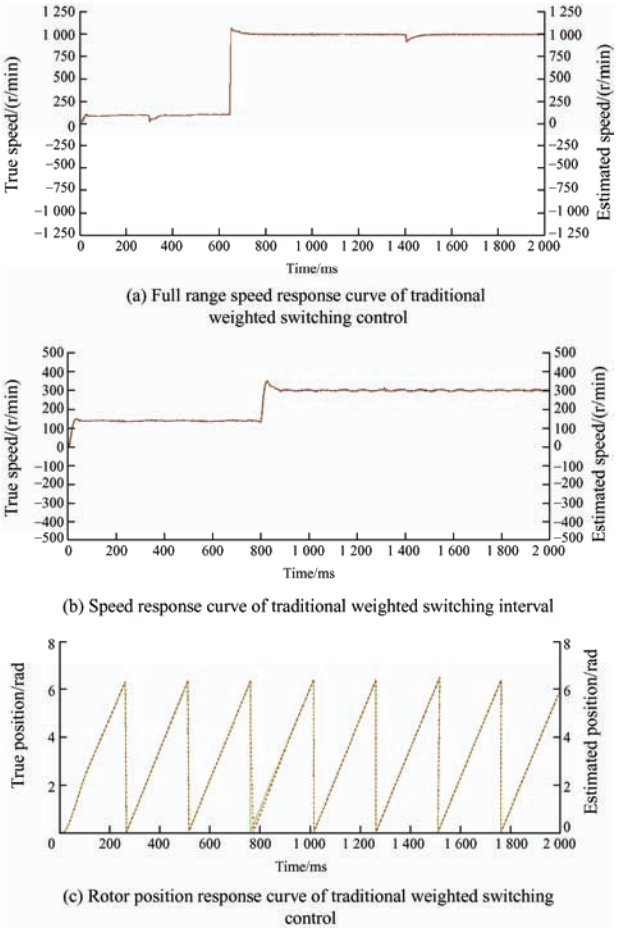

(a) Full range speed response curve of traditional weighted switching control

(b) Speed response curve of traditional weighted switching interval

(c) Rotor position response curve of traditional weighted switching control

Fig. 14 The full range sensorless control waveform under the traditional weighting algorithm

According to the experimental verification, the traditional weighted switching method has a large overshoot under the load.

(2) Under the same working conditions as the traditional algorithm, fuzzy control is carried out in the switching interval according to the waveform of speed and rotor position. The experimental results are shown in Fig. 15.

Compared with the simulation, when the motor speed rises to 1 000 r/min, the reaction time is shorter and the system sensitivity is higher; therefore, overshoot occurs.

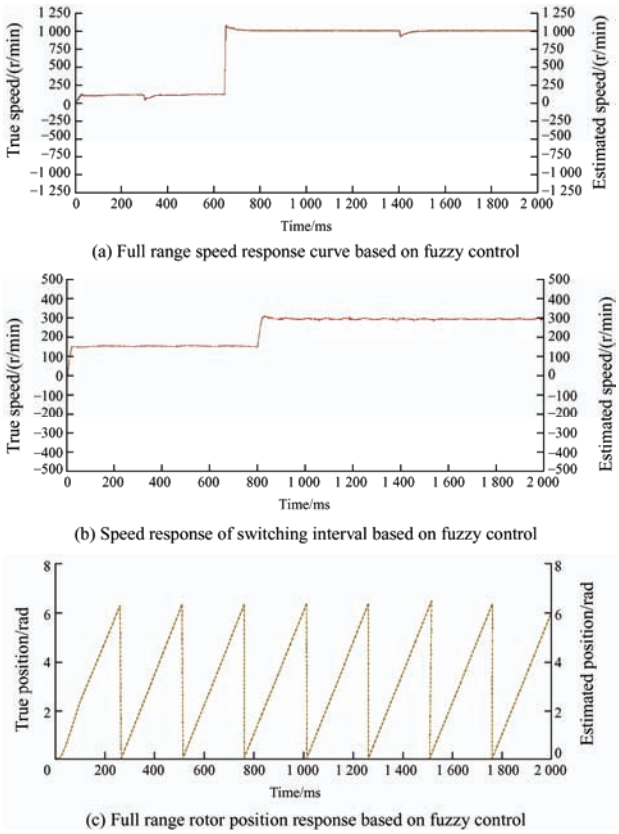

(a) Full range speed response curve based on fuzzy control

(b) Speed response of switching interval based on fuzzy control

(c) Full range rotor position response based on fuzzy control

Fig. 15 Full range sensorless control based on fuzzy control

According to the experimental verification, the fuzzy control algorithm has a smooth transition between the speed and the rotor position in the switching interval. It is verified that the method presents good tracking dynamic performance.

(3) When the motor runs in the full speed range, the traditional speed and rotor position error waveforms, based on weighted switching and fuzzy control, are compared in the switching interval. The experimental results are shown in Fig. 16.

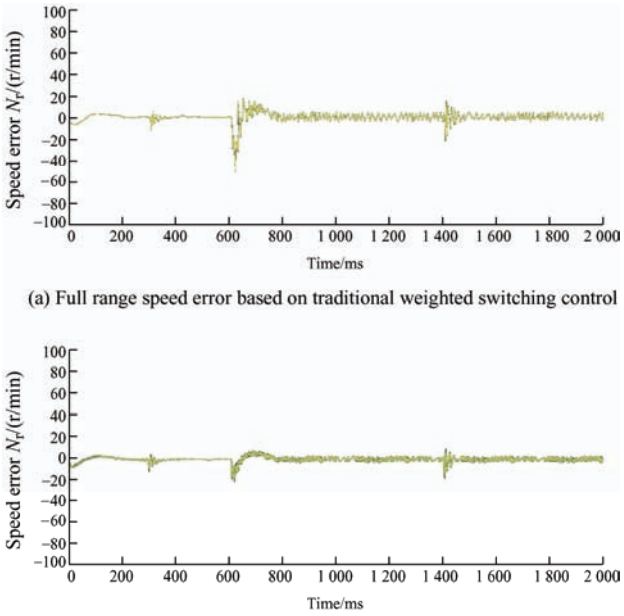

Fig. 16 Comparison of the speed waveforms of the two control algorithms in the switching interval

The experimental results are shown in Fig. 17. The error of traditional weighted switch speed and rotor has obviously increased. Through fuzzy control, it can be seen that the two algorithms can effectively and accurately detect the speed and rotor position in the switching process.

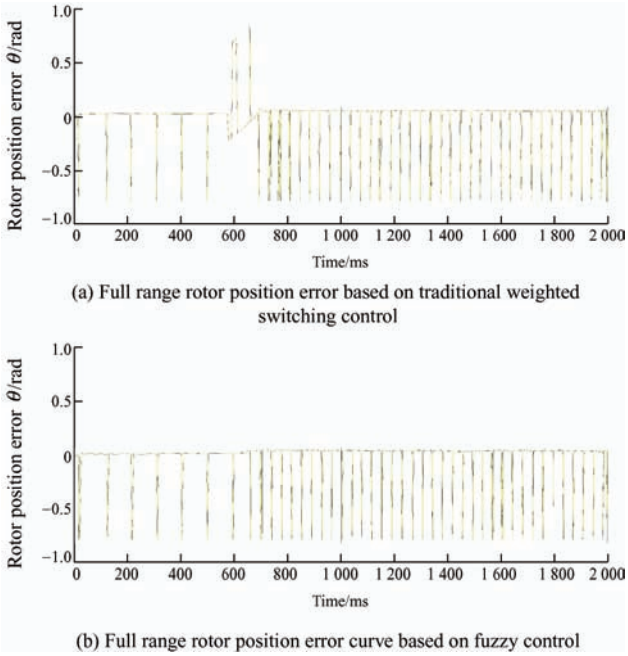

Fig. 17 Comparison of the rotor position waveforms of the two control algorithms in the switching interval

5 Conclusions

In this paper, the overall scheme design and control strategy of the PMSM sensorless control system, are studied, and the control method of motor running in the full-speed range, is analyzed in detail. The simulation results and experiments show that the high-frequency signal injection method in the low-speed range, and the sliding mode observer method in the medium and high speed range, can accurately estimate the rotor position and speed, and the tracking speed is fast. In the estimation process, the robustness improves. At the same time, using fuzzy control in the low-speed to medium and high-speed range, can make the PMSM switch smoothly, which has a certain application value.

References

[1] H Lin, H Guo, H Qian. Design of high-performance permanent magnet synchronous motor for electric aircraft propulsion. *Proc. 21st Int. Conf. Electrfic. Mach. Syst. (ICEMS)*, 2018: 174-179.

[2] S Kim, J I Ha, S K Sul. PWM switching frequency signal injection sensorless method in IPMSM. *IEEE Transactions on Industry Application*, 2012, 48(5): 1576-1587.

[3] Y P Zhou, G Yang, J H Yang. Speed control strategy of permanent magnet synchronous motor based on adaptive backstepping. *Chinese Journal of Electrical Engineering*, 2020, 15(3): 38-43.

[4] Y P Zhou , G Yang , J H Yang. PMSM speed control using adaptive sliding mode control based on an extended state observer. *High Technology Letters*, 2018(4): 422-433.

[5] S Q Peng , Y Y Song . Sensorless vector control of PMSM based on adaptive fuzzy sliding mode observer. *Control and Decision*, 2018, 33(4): 644-648.

[6] A A Hass, A M Elsawy. Sensorless sliding mode torque control of an IPMSM drive based on active flux concept. *Alexandria Engineering Journal*, 2019(51): 1-9.

[7] S Alahakoon, T Fernando, H Trinh, et al. Unknown input sliding mode functional observers with application to sensorless control of permanent magnet synchronous machines. *Journal of the Franklin Institute*, 2013, 350(1): 107-128.

[8] S H Li, Z G Liu. Adaptive speed control for permanent-magnet synchronous motor system with variations of load inertia. *IEEE Transactions on Industrial Electronics*, 2009, 56(8): 3050-3059.

[9] X Q Hu, C Y Sun. Sensorless control of permanent

magnet synchronous motor in full speed range. *Electric Machines & Control Application*, 2016, 20(9): 73-79.

[10] X K Shen. Research on PMSM full speed domain sensorless control technology. Zhengzhou: Zhengzhou University, 2019.

[11] Z Qiao, T Shi, Y Yan, et al. New sliding mode observe for position sensorless control of permanent magnet synchronous motor. *IEEE Trans. Ind. Electron.*, 2017, 60(2): 710-719.

[12] J Yan, S Y Yang, H Y Li . Rotor position estimation for IPMSM based on high frequency rotating voltage injection. *Transactions of China Electrotechnical Society*, 2018, 33(15): 3547-3555.

[13] M N Uddin, M M I Chy. A novel fuzzy logic-controller-based torque and flux controls of IPMSM. *IEEE Transactions on Industria Electronics*, 2020, 46(3): 1220-1229.

[14] D D Wen. Class of pure delay fuzzy-Dahlin control strategy research. *Industrial Instrumentation and Automation*, 2007(4): 3-5.

[15] T Yu, J Liu, W F Sun. Weak magnetic control of permanent magnet synchronous motor based on fuzzy theory. *Chinese Journal of Electrical Engineering*, 2019, 14(1): 1-8.

Dingdou Wen received the B.S. degree in Automation from Nanjing Tech University, Nangjing, China, in 1993, the M.S. degree in Control Theory and Control Engineering from Central South University, Changsha, in 2007.

He has been with Hunan University of Technology, he is currently a Professor of Automatic Control Engineering. His current research interests are permanent magnet synchronous motor speed control.

Wei Wang received his master's degree in Department of Electrical Engineering, Hunan University of Technology, In 2020, Hunan, China. His main research is power electronics and power transmission.

Yang Zhang received his B.S. degree in Applied Physics and his M.S. degree in Electrical Engineering from Hunan University of Technology, Zhuzhou, China. He received his Ph.D. degree in Electrical Engineering from Hunan University, Hunan, China, in 2017. He is currently an Assistant Professor in Hunan University of Technology. His current research interests include wind power generation system and impedance-source converters.